HHS Public Access

Author manuscript

Sci Signal. Author manuscript; available in PMC 2023 November 11.

Published in final edited form as:

Sci Signal. 2023 August 22; 16(799): eadg0661. doi:10.1126/scisignal.adg0661.

Convergent activation of Ca^{2+} permeability in two-pore channel 2 through distinct molecular routes

Ryo Saito[1,2], **Qianru Mu**[1], **Yu Yuan**[1], **Marcos Rubio-Alarcón**[3], **Maria Eznarriaga**[3], **Pingwei Zhao**[4], **Gihan Gunaratne**[5], **Sushil Kumar**[5], **Marco Keller**[6], **Franz Bracher**[6], **Christian Grimm**[7], **Eugen Brailoiu**[4], **Jonathan S. Marchant**[5], **Taufiq Rahman**[3,*], **Sandip Patel**[1,*]

[1]Department of Cell and Developmental Biology, University College London, Gower Street, London WC1E 6BT, UK.

[2]Department of Dermatology, Graduate School of Biomedical and Health Sciences, Hiroshima University, Hiroshima, Japan.

[3]Department of Pharmacology, University of Cambridge, Cambridge, UK.

[4]Center for Substance Abuse Research, Lewis Katz School of Medicine at Temple University, Philadelphia, PA 19140, USA.

[5]Department of Cell Biology, Neurobiology and Anatomy, Medical College of Wisconsin, 8701 Watertown Plank Road, Milwaukee, WI 53226, USA.

[6]Department of Pharmacy—Center for Drug Research, Ludwig-Maximilian University, Munich, Germany.

[7]Walther Straub Institute of Pharmacology and Toxicology, Faculty of Medicine, Ludwig-Maximilians University, Munich, Germany.

Abstract

TPC2 is a pathophysiologically relevant lysosomal ion channel that is activated directly by the phosphoinositide $PI(3,5)P_2$ and indirectly by the calcium ion (Ca^{2+})–mobilizing molecule NAADP through accessory proteins that associate with the channel. TPC2 toggles between $PI(3,5)P_2$-induced, sodium ion (Na^+)–selective and NAADP-induced, Ca^{2+}–permeable states in response to these cues. To address the molecular basis of polymodal gating and ion-selectivity

*Corresponding author. mtur2@cam.ac.uk (T.R.); patel.s@ucl.ac.uk (S.P.).

Author contributions: R.S. and Q.M. performed the Western blotting. Q.M. and Y.Y. performed the immunocytochemistry and confocal microscopy. R.S. and Y.Y. performed the Ca^{2+} imaging. S.P. designed the plasmids. M.R.-A., M.E., and T.R. performed the electrophysiology. P.Z. and E.B. performed the microinjection and associated Ca^{2+} imaging. G.G., S.K., and J.S.M. developed the knockout cells. M.K., F.B., and C.G. designed and synthesized the TPC2 agonists. S.P., T.R., and J.S.M. conceived the study. S.P. wrote the manuscript in consultation with all coauthors.

Supplementary Materials
This PDF file includes:
Figs. S1 to S7
Table S1

Other Supplementary Material for this manuscript includes the following: MDAR Reproducibility Checklist

Competing interests: The authors declare that they have no competing interests.

Data and materials availability: All data needed to evaluate the conclusions in the paper are present in the paper or the Supplementary Materials. Materials are available upon reasonable request.

switching, we investigated the mechanism by which NAADP and its synthetic functional agonist, TPC2-A1-N, induced Ca^{2+} release through TPC2 in human cells. Whereas NAADP required the NAADP-binding proteins JPT2 and LSM12 to evoke endogenous calcium ion signals, TPC2-A1-N did not. Residues in TPC2 that bind to $PI(3,5)P_2$ were required for channel activation by NAADP but not for activation by TPC2-A1-N. The cryptic voltage-sensing region of TPC2 was required for the actions of TPC2-A1-N and $PI(3,5)P_2$ but not for those of NAADP. These data mechanistically distinguish natural and synthetic agonist action at TPC2 despite convergent effects on Ca^{2+} permeability and delineate a route for pharmacologically correcting impaired NAADP-evoked Ca^{2+} signals.

INTRODUCTION

Nicotinic acid adenine dinucleotide phosphate (NAADP) is a potent Ca^{2+}-mobilizing messenger produced in response to diverse extracellular cues to regulate numerous Ca^{2+}-dependent outputs from fertilization to differentiation and beyond (1). In most systems, it stimulates the release of Ca^{2+} from acidic organelles through two-pore channels (TPCs) (2–6), which are ancient members of the voltage-gated ion channel superfamily that localize to acidic organelles (6–10). TPCs play prominent evolutionarily conserved roles in organellar architecture, such as membrane contact site formation and vesicular trafficking, and they are implicated in a number of disorders, including Parkinson disease, liver dysfunction, viral infection, and cancer (10–15).

However, despite the clear importance of NAADP and TPCs, the molecular relationship between the two is unresolved (16). TPCs do not bind NAADP. Instead, NAADP binds to small–molecular weight proteins that associate with TPCs (17–20). We and others converged on Jupiter microtubule associated homolog (JPT2) as the long-sought NAADP receptor that mediates the effect of NAADP on TPCs (21, 22). JPT2 selectively binds NAADP, associates with TPCs, and is required for NAADP-mediated Ca^{2+} signaling and viral trafficking (21). Other studies identified a second distinct NAADP receptor, like-Sm protein 12 (LSM12), which also appears necessary for NAADP-mediated Ca^{2+} signaling (23). The relationship between JPT2 and LSM12 in NAADP action requires definition (24, 25).

In addition to NAADP, TPCs are activated directly by the endolysosomal-enriched phosphoinositide, phosphatidylinositol 3,5-bisphosphate [$PI(3,5)P_2$] (26) through a structurally resolved binding site (27, 28). $PI(3,5)P_2$ induces largely Na^+-selective currents through both TPC1 (29) and TPC2 (26). This is in contrast to a body of literature indicating TPCs are nonselective cation channels gated by NAADP (8, 30, 31). Parallel analyses of TPC2 in the presence of NAADP or $PI(3,5)P_2$ confirmed this divergent ion selectivity profile and identified small-molecule activators of TPC2 that mimic these effects (32). Additional analyses show that despite the radically different actions of NAADP, $PI(3,5)P_2$, and their mimetics on TPC2 permeability, they synergize to increase Ca^{2+} but not Na^+ flux (33). This leads to a paradigm in which an ion channel can switch its permeability in an agonist-dependent manner to independently control cation flux and associated downstream functions, such as lysosomal pH, motility, and exocytosis. The interplay between indirect

and direct control of TPC activity is currently undefined and is important to establish to effectively target the channel with drugs.

Here, we probed the role of NAADP-binding proteins, the $PI(3,5)P_2$ binding site, and the voltage-sensing region in agonist activation of TPC2. We distinguished the actions of NAADP from those of a functional mimetic, thereby revealing how the Ca^{2+} signaling modality of TPC2 can be achieved through distinct means. These data revealed mechanistic insight into polymodal gating and suggest a strategy for correcting deviant NAADP-mediated Ca^{2+} signals.

RESULTS

The NAADP mimetic TPC2-A1-N mediates Ca^{2+} signals independently of NAADP-binding proteins

In the accompanying study (34), we revealed a dual requirement for JPT2 and LSM12 in NAADP signaling through TPCs. Here, we tested the requirement for these NAADP-binding proteins in the actions of TPC2-A1-N, a small-molecule activator of TPC2 that mimics the Ca^{2+} signaling modality of NAADP but is not a structural analog of NAADP (32). We used haploid HAP1 and diploid U2OS knockout cells lacking JPT2, LSM12, or both.

Western blot analyses using antibodies specific for JPT2 or LSM12 identified proteins of ~25 kDa in control cells but no detectable signals in each of the respective knockouts or the double-knockout cells (Fig. 1A and fig. S1, A to C). To further validate these cells, we performed immunocytochemical analysis with the same antibodies. We noted largely diffuse staining throughout the cytosol for both NAADP-binding proteins in control HAP1 cells, and staining was absent in the respective knockout cell lines (Fig. 1B). Immunocytochemistry in mock-edited U2OS cells showed that JPT2 staining was largely diffuse, as in the HAP1 cells, and specific because it was not evident in the knockout cells (Fig. 1C). This analysis, however, revealed a punctate distribution for LSM12 in U2OS cells (Fig. 1C and fig. S1D). To investigate the subcellular location of NAADP-binding proteins in U2OS cells, we costained cells with an antibody to the late-endosome and lysosomal protein, LAMP1. Whereas a portion of the LSM12 puncta colocalized with LAMP1 puncta, there was minimal overlap of JPT2 with LAMP1 (Fig. 1D). Upon enlargement of lysosomes by vacuolin treatment, large LAMP1-positive vacuoles were readily identifiable, and a proportion of them were also positive for LSM12 (Fig. 1D).

To test the requirement for JPT2 and LSM12 proteins in TPC2-A1-N action, we first examined the effect of TPC2-A1-N on endogenous TPC2-mediated Ca^{2+} signals in HAP1 cells using the fluorescent ratiometric Ca^{2+}-sensitive indicator Fura-2. TPC2-A1-N evoked a detectable response that was largely unaffected by knockout of LSM12 or JPT2, but these signals were small in amplitude (fig. S2A). To better characterize TPC2-dependent Ca^{2+} signals, we leveraged our previous findings showing that TPC2-A1-N synergizes with a $PI(3,5)P_2$ functional mimetic, TPC2-A1-P, to selectively increase the Ca^{2+} permeability of TPC2 (33). HAP1 cells were therefore stimulated with a combination of TPC2-A1-N and TPC2-A1-P. The combination induced a larger Ca^{2+} response in control HAP1 cells (Fig. 2A) than either mimetic alone (fig. S2, A and B). This response was unaffected by knockout

of either JPT2 or LSM12 (Fig. 2A), thereby distinguishing the effects of TPC2-A1-N and NAADP.

In an independent approach, we examined the effects of TPC2-A1-N in diploid U2OS cells. In this cell type, TPC2-A1-N alone evoked a larger response than that in HAP1 cells (Fig. 2B). The responses were similar in mock knockout, LSM12 knockout, and JPT2 knockout cells, providing further evidence that the effects of TPC2-A1-N were independent of NAADP receptors (Fig. 2B). Essentially, similar results were obtained using TPC2-A1-N in combination with TPC2-A1-P (fig. S3, A and B). To test for possible compensation between NAADP-binding proteins upon knockout, we analyzed the effects of TPC2-A1-N in double-knockout cells lacking both LSM12 and JPT2. As with the single knockouts, there was little effect on Ca^{2+} signals evoked by TPC2-A1-N (Fig. 2C) or TPC2-A1-N in combination with TPC2-A1-P (fig. S3, C and D). In a converse approach, we examined the effect of LSM12 and JPT2 overexpression on Ca^{2+} signals evoked by TPC2-A1-N. Neither of the proteins, when overexpressed, affected endogenous Ca^{2+} signals evoked by TPC2-A1-N (Fig. 2D). Overexpression of LSM12 modestly reduced the response to the agonist combination, but JPT2 overexpression was without effect (Fig. 2D and fig. S4). Overall, these data show that TPC2-A1-N responses were independent of NAADP-binding protein amounts.

We also examined the requirement for LSM12 and JPT2 on activation of recombinant TPC2 by TPC2-A1-N using two approaches. In the first, we expressed TPC2 fused to the fluorescent Ca^{2+} indicator protein GCaMP6s at its cytosolic C terminus in double-knockout U2OS cells to record lysosomal Ca^{2+} release (Fig. 2E). In the second, we expressed TPC2 rerouted to the plasma membrane by mutating the N-terminal lysosomal targeting sequence ($TPC2^{L11A/L12A}$) to record Ca^{2+} influx (Fig. 2F). TPC2-A1-N evoked robust Ca^{2+} signals in both cases, and these responses were not different upon dual knockout of the NAADP-binding proteins (Fig. 2, E and F). Essentially, similar results were obtained in influx assays upon single knockout of the NAADP-binding proteins (fig. S5, A and B). In summary, using both knockout and overexpression approaches, we showed that TPC2-A1-N activated TPC2 independently of the NAADP-binding proteins JPT2 and LSM12 despite having similar effects to NAADP on channel permeability.

Activation of TPC2 by NAADP requires the $PI(3,5)P_2$ binding site

NAADP and $PI(3,5)P_2$ have disparate effects on the permeability of TPC2 but appear to work synergistically (33, 35), suggesting that their actions are in some way linked. To probe the relationship between NAADP and $PI(3,5)P_2$, we examined the effects of mutating the $PI(3,5)P_2$ binding site on agonist action. $PI(3,5)P_2$ binds to TPC2 by bridging residues in the S4-S5 linker and S6 helix in the first domain (Fig. 3A) (28). We mutated essential lysine residues Lys^{204} or Lys^{207} in the linker (K204A and K207A) in $TPC2^{L11A/L12A}$ to reroute channels to the plasma membrane for patch clamp analyses. Human embryonic kidney (HEK) cells transiently expressing $TPC2^{L11A/L12A}$ at the cell surface supported robust currents in response to $PI(3,5)P_2$ using symmetrical Na^+ solutions (Fig. 3B). Mutation of either Lys^{204} or Lys^{207} caused substantial inhibition of the $PI(3,5)P_2$-evoked currents (Fig. 3B), as reported previously (28). NAADP also robustly activated $TPC2^{L11A/L12A}$ in the

plasma membrane (Fig. 3C). These currents were blocked by the pore blocker raloxifene and not detected in cells expressing TPC2 mutated within the pore (fig. S6A), consistent with previous analyses (8, 36). The K204A and K207A mutations also abolished the NAADP currents (Fig. 3C).

To further investigate the relationship between NAADP and $PI(3,5)P_2$, we mutated residues in the S6 helix of TPC2. $PI(3,5)P_2$ interacts with Arg^{329} in the S6 extension in the closed state and undergoes structural rearrangements and additional interaction with Ser^{322} in the open state (Fig. 3D) (28). Mutation of Arg^{329} or Ser^{322} inhibited $PI(3,5)P_2$-mediated currents (Fig. 3E), as reported (28). In addition, as with the linker mutations, they also abolished NAADP action (Fig. 3F).

We also analyzed NAADP-mediated Ca^{2+} signals in intact U2OS cells expressing lysosomal wild-type TPC2 or $TPC2^{K204A}$. In these experiments, NAADP was delivered by pressure microinjection. NAADP evoked a prompt Ca^{2+} signal in Fura-2–loaded cells expressing wild-type TPC2, but there was little response in cells expressing $TPC2^{K204A}$ (Fig. 3G), consistent with reduced currents. Together, these experiments demonstrate that, despite the indirect effects of NAADP and direct effects of $PI(3,5)P_2$ on TPC2, they share common molecular determinants for channel activation.

Activation of TPC2 by TPC2-A1-N is independent of $PI(3,5)P_2$ binding

We next probed the requirement of the $PI(3,5)P_2$ binding site for channel activation by TPC2-A1-N as assayed by patch clamping in HEK cells. TPC2-A1-N induced currents through $TPC2^{L11A/L12A}$ (Fig. 4A) that were comparable in magnitude to those mediated by NAADP (Fig. 3C). Similar to NAADP, they were blocked by raloxifene or by mutation of the pore (fig. S6B). However, in contrast to the NAADP- and $PI(3,5)P_2$-evoked currents, currents evoked by TPC2-A1-N were unaffected by mutation of Lys^{204} and Lys^{207} within the S4-S5 linker (Fig. 4A). Mutation of Arg^{329} and Ser^{322} in the S6 extension also failed to affect the currents (Fig. 4A). In these experiments, TPC2-A1-N evoked currents in all 13 patches tested. However, in four of those patches, NAADP failed to evoke a current (Fig. 4B), again distinguishing the actions of NAADP and TPC2-A1-N. Comparison of the TPC2-A1-N currents in NAADP-sensitive and -insensitive patches showed no difference in amplitude (Fig. 4C).

In an independent approach to assessing TPC2-A1-N action, we measured Ca^{2+} influx through TPC2 at the plasma membrane in HeLa cells loaded with Fura-2. TPC2-A1-N evoked prompt Ca^{2+} influx in cells expressing $TPC2^{L11A/L12A}$ (Fig. 4D). Mutagenesis of the S4-S5 linker or S6 had relatively little effect on Ca^{2+} influx (Fig. 4D) consistent with the electrophysiology (Fig. 4A). We also measured Ca^{2+} release in cells expressing TPC2-GCaMP6s and without the various mutations (Fig. 4E). Again, as with $TPC2^{L11A/L12A}$, mutagenesis of the $PI(3,5)P_2$ binding site had little effect on the TPC2-A1-N activity (Fig. 4E).

Last, we tested the requirement for $PI(3,5)P_2$ in TPC2-A1-N activation of endogenous TPC2 by blocking synthesis of $PI(3,5)P_2$ in HeLa cells with the PIKfyve inhibitor apilimod. Apilimod did not affect the Ca^{2+} responses evoked by TPC2-A1-N (Fig. 4F). Consistent

with depletion of $PI(3,5)P_2$, it caused vacuole formation and enlarged LAMP1-positve structures (Fig. 4G). Together, these data (summarized in Fig. 4, H to J) show that activation of TPC2 by TPC2-A1-N was $PI(3,5)P_2$ independent. This provides additional evidence that TPC2-A1-N actions are distinct from those of NAADP despite phenocopying the effects of NAADP on Ca^{2+} permeability.

Residues outside the $PI(3,5)P_2$ binding site are required for NAADP and TPC2-A1-N actions

To further probe the molecular determinants of agonist action, we mutated residues in TPC2 not implicated in $PI(3,5)P_2$ binding. We focused on Trp^{211} in the S4-S5 linker, which is downstream of the polybasic region (Fig. 5A). In these experiments, we recorded currents through $TPC2^{L11A/L12A}$ in HEK cells under bi-ionic conditions with Ca^{2+} in the pipette solution (corresponding to extracellular space or lysosome lumen) and Na^+ in the bath (corresponding to the cytosol). The reversal potential (E_{rev}) for currents evoked by NAADP was −10 ± 0.4 mV, corresponding to a P_{Ca}/P_{Na} of ~0.6, similar to that reported previously (32). Mutation of Trp^{211} to Ala (W211A) blocked both outward (Na^+) currents and inward (Ca^{2+}) currents (Fig. 5, B to D). TPC2-A1-N evoked similar currents to those evoked by NAADP in control cells expressing $TPC2^{L11A/L12A}$ with an E_{rev} of −13 ± 1 mV, and, similar to NAADP, TPC2-A1-N–evoked currents were blocked in cells expressing $TPC2^{L11A/L12A/W211A}$ (Fig. 5, B to D). We also examined the effects of Trp^{211} on currents evoked by $PI(3,5)P_2$. $PI(3,5)P_2$ evoked robust currents with a negatively shifted E_{rev} (−67 ± 5 mV) corresponding to a P_{Ca}/P_{Na} of ~0.04. $PI(3,5)P_2$-evoked currents were also blocked by the W211A mutation despite lack of direct contact of $PI(3,5)P_2$ with Trp^{211} (Fig. 5, B to D). Thus, Trp^{211} is a common determinant for activation of TPC2 by NAADP, TPC2-A1-N, and $PI(3,5)P_2$. This was not due to aberrant trafficking of the mutant forms of plasma membrane–targeted TPC2 because confocal analyses revealed similar subcellular distributions for $TPC2^{L11A/L12A}$ and $TPC2^{L11A/L12A/W211A}$ (fig. S7). In a related set of experiments, we examined the effects of mutating Arg^{331}. This residue is in the S6 extension and downstream of residues that coordinate the $PI(3,5)P_2$ head group during channel opening (Fig. 5A). Currents evoked by all three TPC2 agonists were reduced for the R331A mutant similar to W211A (Fig. 5, B to D). Again, the Arg^{331}mutant appeared to traffic normally (fig. S7).

In an independent approach, we examined the effects of the mutations on Ca^{2+} influx by rerouted TPC2 in response to TPC2-A1-N. Influx of Ca^{2+} in cells expressing $TPC2^{L11A/L12A/W211A}$ or $TPC2^{L11A/L12A/R331A}$ was largely reduced (Fig. 5E), consistent with reduced Ca^{2+} currents. Essentially, similar results were obtained in lysosomal Ca^{2+} release assays (Fig. 5F). Thus, mutation of either Trp^{211} or Arg^{331} in TPC2-GCaMP6s reduced Ca^{2+} responses to TPC2-A1-N.

To further identify residues that are important for agonist action, we considered the voltage-sensing region in domain II of TPC2. Activation of TPC1 by $PI(3,5)P_2$ is voltage-sensitive, but activation of TPC2 is not due to the absence of a positively charged voltage-sensing residue in S4 of domain II (28). Nevertheless, downstream arginine residues within S4 are conserved, suggesting an important role in channel function, and tricyclic antidepressants reveal voltage-dependent activation of TPC2 (37). We therefore mutated Arg^{557} in S4 (Fig.

5G) to alanine (R557A) and examined its effects on agonist action. Patch clamp analyses of HEK cells expressing $TPC2^{L11A/L12A/R557A}$ showed that the NAADP-evoked currents were similar to cells expressing the wild-type channel (Fig. 5H). In stark contrast, currents evoked by TPC2-A1-N were substantially reduced (Fig. 5H). Essentially, similar results were obtained with $PI(3,5)P_2$ (Fig. 5H). Regarding the effects of the R557A mutation on TPC2-A1-N–mediated Ca^{2+} influx, Ca^{2+} signals evoked by TPC2-A1-N were reduced (Fig. 5I), again distinguishing the activation of TPC2 by NAADP versus TPC2-A1-N. To further validate these findings, we examined the effect of TPC-A1-N–evoked Ca^{2+} release in cells expressing $TPC2^{R557A}$-GCaMP6s. Responses were delayed relative to cells expressing TPC2-GCaMP6s (Fig. 5J), consistent with abrogated channel activity. Together, these electrophysiological and imaging analyses (summarized in Fig. 5K) identify key residues remote from the $PI(3,5)P_2$ binding site that are essential for all agonist activation of TPC2 and a role for the S4 voltage sensor in mediating agonist-selective activation of TPC2.

DISCUSSION

TPC2 is a highly unusual ion channel able to switch its permeability in an agonist-dependent manner (32, 33). Here, we identified key molecular determinants mediating TPC2 activation. We showed how the same channel outcome (Ca^{2+} permeability) mediated by NAADP and by an NAADP mimetic was achieved through different molecular determinants. Polymodal activation of TPC2 thus proceeds through divergent routes (Fig. 5L).

NAADP has long been known to activate TPCs indirectly based on photo-affinity labeling experiments (17–20). The eagerly awaited identification of NAADP receptors that associate with TPCs (21, 23) rationalizes NAADP action within a receptor-channel complex (18). As shown in the accompanying manuscript (34), both JPT2 and LSM12 are direct targets for NAADP, and both are required for NAADP-mediated Ca^{2+} signaling. Our immunocytochemical studies (Fig. 1, C to D) revealed cell type–specific differences in the localization of these endogenous NAADP-binding proteins. In particular, the distribution of JPT2 and LSM12 appears more punctate in U2OS cells than in HAP1 cells, with greater colocalization of LSM12 with lysosomes. This is consistent with LSM12 preferentially associating with TPC2 over TPC1 (34).

Biophysically, NAADP and the small-molecule agonist TPC2-A1-N evoke almost identical currents through TPC2 (32, 33). TPC2-A1-N is selective for TPC2 over TPC1 and TRPML1 (32), but its molecular mechanism of action has not been characterized. We demonstrated four properties that distinguish NAADP and TPC2-A1-N: First, only NAADP-evoked Ca^{2+} signals were blocked by knockout of JPT2 and/or LSM12 (Fig. 2, A to F) (34); second, only NAADP-evoked channel activation was blocked by mutation of the $PI(3,5)P_2$ binding site in TPC2 (Figs. 3, C and F; and 4, A to E); third, TPC2-A1-N activated TPC2 in NAADP-insensitive patches of cellular membranes (Fig. 4B); and, fourth, only TPC2-A1-N–induced channel activation was blocked by mutation of the voltage sensor in TPC2 (Fig. 5, H to K). These data divorce the actions of the agonists. They also point to TPC2 as likely a direct target for TPC2-A1-N, explaining why TPC2-A1-N is a more consistent channel activator than NAADP, which targets TPC2 indirectly through NAADP-binding proteins. Perhaps

most notably, our results show how the convergent actions of these two "Ca^{2+} agonists" on TPC2 permeability are mediated by distinct molecular mechanisms.

$PI(3,5)P_2$ interaction with TPC2 is detailed at the atomic level with cryo–electron microscopy (cryo-EM) structures available in both agonist-bound closed and agonist-bound open states (28). Our data showing marked convergence on $PI(3,5)P_2$-interacting residues for NAADP and $PI(3,5)P_2$ were unexpected, given that NAADP does not bind TPCs. This requirement was strict, spanning the S4-S5 linker and S6 helix in domain I (Fig. 3, A to F), but evidently selective, given that TPC2-A1-N responses were unperturbed when these residues were mutated (Fig. 4, A to E). NAADP and $PI(3,5)P_2$ synergize to activate TPC2 (33, 35), consistent with them acting at distinct sites. It is unlikely that the inhibition of NAADP action we observed by abrogating the $PI(3,5)P_2$ site was due to antagonism of endogenous $PI(3,5)P_2$ because our electrophysiological measurements were performed with TPC2 redirected to the plasma membrane, where $PI(3,5)P_2$ abundance is low. We speculate that these mutations, as well as disrupting $PI(3,5)P_2$ binding, induce structural changes that perturb the NAADP-binding protein–channel interface. This mechanism is likely conserved across TPC homologs because previous studies with TPC1 showed that mutation of the S4-S5 linker abrogated NAADP-induced Ca^{2+} release (38), although direct channel activity was not reported.

Channel opening is associated with ordering of the S4-S5 linker in domain II (28). Our data uncover the preceding S4 region where Arg^{557} resides as a key determinant of channel activation by TPC2-A1-N (Fig. 5, H to K). Although TPC2 is considered voltage-insensitive, as evidenced by linear current-voltage relationships for $PI(3,5)P_2$ as well as for NAADP and TPC2-A1-N (Fig. 3, A to F), a number of tricyclic antidepressants activate the channel in a voltage-sensitive manner (37). This points to "cryptic" voltage sensing by TPC2, most likely through the voltage sensor domain in domain II (39), which, although normally nonfunctional, can support voltage-sensitive $PI(3,5)P_2$ currents upon introduction of an arginine residue at the R3 position (I551R) (28). Thus, this region emerges as hub for channel activation by both voltage-sensitive and -insensitive activators. R557A also blocked channel activation by $PI(3,5)P_2$. This convergence of $PI(3,5)P_2$ with TPC2-A1-N in the voltage sensor together with NAADP in the S4-S5 linker demonstrates how a different channel outcome (selectivity switching) is achieved through the same molecular determinants. However, it is the bypass of the blocking effects of R557A by NAADP that is ostensibly the more informative. Not only does this form part of the evidence distinguishing the action of NAADP from that of TPC2-A1-N, but it also suggests that the interaction of NAADP binding proteins with TPCs phenocopies the presumed conformational changes in the voltage-sensor region evoked by TPC2-A1-N. Different mechanisms for switching ion selectivity thus likely exist.

Additional mutagenesis using our three-pronged approach combining electrophysiology, Ca^{2+} influx, and Ca^{2+} release identified the importance of Trp^{211} and Arg^{331} for channel activation (Fig. 5, A to F). Neither residue contacts $PI(3,5)P_2$ in available TPC2 structures (28). Nevertheless, they are required for activation of TPC2 by $PI(3,5)P_2$ as well as by NAADP and TPC2-A1-N. We interpret this remoteness and pan-inhibition to indicate a role for these residues in transducing ligand binding events (regardless of agonist) to pore

opening. This highlights the region straddling the S4-S5 linker and the S6 helix as an "integrator" of agonist action.

Pharmacological, molecular, and genetic approaches have identified numerous functional roles for TPC2 that have been mostly ascribed to NAADP action, for example, in vesicular (13) and non-vesicular (14) membrane traffic. One implication of dissociating the effects of NAADP and TPC2-A1-N action reported here is that the latter could be used to correct NAADP signaling deficiency in disease states. In cases where the deficit is caused by failure of the NAADP-binding proteins to bind NAADP or to interact with TPCs, our observation that TPC2-A1-N evoked Ca^{2+} responses in cells lacking NAADP-binding proteins (Fig. 2, A to F) suggests that TPC2-A1-N may be useful for rescuing the loss of NAADP-evoked Ca^{2+} signals. TPC2-A1-N may also be useful in contexts in which more distal defects may impair NAADP-evoked Ca^{2+} release, for example, deficiencies in enzymes, such as CD38, SARM1, and/or DUOX, that promote NAADP synthesis and play roles in immune dysfunction and neurodegeneration (40). The ability of TPC2-A1-P to promote autophagy and lysosomal exocytosis has been leveraged to revert lysosomal storage phenotypes in vitro and in vivo (41). Because TPC2 is activated by both NAADP and $PI(3,5)P_2$ and coupled to distinct functionally relevant ionic profiles, it is difficult to unequivocally ascribe phenotypic change upon TPC2 blockade to a specific activation pathway. The pronounced agonist-selective block reported here for the R557A mutant provides a tractable experimental means for dissociating NAADP and $PI(3,5)P_2$ action. In summary, we have provided key insights into how TPC2 is activated in a polymodal manner by identifying molecular determinants underpinning agonist action and associated Ca^{2+} permeability.

MATERIALS AND METHODS

Chemicals

TPC2-A1-N and TPC2-A1-P were synthesized as described previously (32). All other reagents were from Sigma-Aldrich unless otherwise stated.

Cells

HeLa cells, U2OS cells (mock knockout or JPT2 and/or LSM12 knockout) (34), and HEK-293T cells (American Type Culture Collection: CRL-3216 up to passage 20) were maintained in Dulbecco's modified Eagle medium, supplemented with 10% fetal bovine serum (FBS), streptomycin (100 μg/ml), and penicillin (100 U/ml) (all from Invitrogen) at 37°C in a humidified atmosphere with 5% CO_2. HAP1 cells (parental or JPT2/LSM12 knockout) (34) were maintained in Iscove's modified Dulbecco's medium, supplemented with 10% FBS, streptomycin (100 μg/ml), and penicillin (100 U/ml) (all from Invitrogen) at 37°C in a humidified atmosphere with 5% CO_2. These lines are not commonly misidentified. Cells were passaged with trypsin. Cells were plated onto coverslips coated with poly-L-lysine (20 to 100 μg/ml) for immunocytochemistry, epifluorescence imaging, and electrophysiology.

Plasmids

Plasmid encoding human JPT2 (accession: Q9H910–3) and LSM12 (accession: Q3MHD2) were generated by gene synthesis and cloned into the Xho I and Apa I restriction sites of pcDNA3.1(+)-C-Myc and the Bam HI and Eco RI restriction sites of pcDNA3.1(+)-C-DYK, respectively. The coding sequences incorporating a 3' (Gly-Ser-Ala)3 flexible linker were subcloned into pcDNA3-mRuby2 (Addgene plasmid #40260) (42) by homologous recombination using the primer sequences listed in table S1. All gene synthesis and subcloning were performed by GenScript (Piscataway, NJ).

TPC2-expressing plasmids were based on TPC2 mRFP (4), TPC2-GCaMP6s (32), and $TPC2^{L11A/L12A}$–GFP (8). Additional mutations were introduced by site-directed mutagenesis using the primers listed in table S1. $TPC2^{L11A/L12A/L265P}$-GFP was described in (8). TPC2L11A/L12A/K204A-GFP and TPC2L11A/L12A/K207A-GFP were gifts from Jiang and colleagues (43). Cells were transiently transfected with plasmids 18 to 26 hours (U2OS or HeLa) before imaging or 24 to 36 hours (HEK-293T) before electrophysiology, using Lipofectamine 2000 (from Invitrogen) according to the manufacturer's instructions.

Western blotting

Cells were harvested with trypsin, washed once with phosphate-buffered saline by centrifugation, and lysed in phosphate-buffered saline containing 1% Triton X-100 (Sigma-Aldrich) and Halt protease and phosphatase inhibitor cocktail (from Thermo Fisher Scientific) for 30 min at 4°C with rotation. The supernatant was collected after centrifugation (16,000*g* for 10 min at 4°C). The protein concentrations were measured using bicinchoninic acid and bovine serum albumin protein standards. The cell lysates (31 μg) were separated on NuPAGE 12% Bis-Tris Protein Gels (from Invitrogen) and transferred to nitrocellulose membranes according to the manufacturer's instructions (iBlot2 dry blotting system, Invitrogen). The membranes were then blocked with 5% (w/v) dried skimmed milk in tris-buffered saline (from Merck) containing 0.1% (v/v) Tween 20 (TBS-T) for 1 hour at room temperature. Blots were sequentially incubated with primary and secondary antibodies in TBS-T supplemented with 2.5% (w/v) dried skimmed milk. The primary antibodies used were anti-JPT2 (rabbit, HPA041908, Sigma-Aldrich; 1 in 4000, overnight at 4°C), anti-LSM12 (mouse, Proteintech; 1 in 5000, overnight at 4°C), and anti–β-actin (mouse, Proteintech; 1 in 10,000, for 1 hour at room temperature). Secondary antibodies used were IRDye 680RD donkey anti-rabbit immunoglobulin G (IgG) and IRDye 800CW donkey anti-mouse IgG (both from LiCor; 1 in 14000, for 1 hour at room temperature). The fluorescence was detected using Odyssey CLx (LiCor), and images were analyzed using Image Studio Lite version 5.2.

Immunocytochemistry

Immunocytochemistry was performed using the protocol described previously (44) except that coverslips were mounted onto microscope slides using Fluoromount-G (Thermo Fisher Scientific) in place of DABCO. Briefly, cells were fixed with paraformaldehyde, permeabilized with β-escin, blocked with bovine serum albumin/FBS and sequentially incubated with antibodies and 4',6-diamidino-2-phenylindole (DAPI) with intervening washes with Tween 20. Primary antibodies used were rabbit anti-LSM12 antibody (1:100

dilution; catalog no. ab173291 from Abcam), rabbit anti-JPT2 antibody (1:100 dilution; catalog no. HPA041908 from Sigma-Aldrich), and/or mouse anti-LAMP1 antibody (H4A3) (1:10 dilution, Developmental Studies Hybridoma Bank). Secondary antibodies used were goat anti-rabbit (Alexa Fluor 488; 1:100 dilution; catalog no. 50077 from Abcam) and/or donkey anti-mouse (Alexa Fluor 594; 1:100 dilution; catalog no. A21203 from Thermo Fisher Scientific).

Confocal microscopy

Confocal images were captured using a Zeiss 880 axio observer Z1, fitted with Plan-Apochromat 63×/1.4 oil differential interference contrast objective. DAPI, GFP, and Alexa Fluor 594 fluorescence were excited using wavelengths of 405, 488, and 594 nm, respectively. Emitted fluorescence was captured using 410- to 479-nm, 490- to 577-nm, or 578- to 696-nm band-pass filters, respectively. Confocal images were analyzed using Fiji software.

Single-cell Ca^{2+} measurements

Cytosolic Ca^{2+} was measured at the single-cell level using the fluorescent dye Fura-2 (from Biotium) or the genetically encoded Ca^{2+} indicator GCaMP6s fused to the C terminus of TPC2 (32). Ca^{2+} imaging experiments were performed at room temperature in Hepes-buffered saline (HBS) containing 10 mM Na Hepes, 1.25 mM KH_2PO_4, 2 mM $MgSO_4$, 3 mM KCl, 156 mM NaCl, 2 mM $CaCl_2$, and 10 mM glucose (pH 7.4). For dye loading, cells were incubated with Fura-2 AM (2.5 μM) and 0.005% (v/v) pluronic acid (from Invitrogen) for 1 hour in HBS.

After transfection and/or dye loading, cells were washed in HBS and were subsequently mounted in a 1-ml imaging chamber (Bioscience Tools) for microscopy. Epifluorescence images were acquired every 3 s. For Fura-2 measurements, images were captured with a cooled coupled device camera (TILL Photonics) attached to an Olympus IX71 inverted fluorescence microscope fitted with a monochromatic light source under the control of TillVision 4.0 software. Fura-2 was excited at 340/380 nm, and emitted fluorescence was captured using a 440-nm long-pass filter at ×20 or ×40 magnification. For GCaMP6s measurements, images were captured using a megapixel monochrome cooled coupled device camera attached to an Olympus IX73 inverted fluorescence microscope fitted with a CoolLED multiple wavelength light-emitting diode source under the control of MetaFluor 7.10.3.279 software.

Cells were stimulated with TPC2-A1-N (30 μM) and TPC2-A1-P (60 μM) either alone or in combination. Where indicated, some experiments were performed in Ca^{2+}-free HBS where $CaCl_2$ was omitted, and the cells were stimulated with ionomycin (2 μM Ca^{2+} salt; Cayman Chemical) toward the end of the recording period.

Ca^{2+} measurements upon microinjection of NAADP were performed as described in the accompanying paper (34). Briefly, U2OS cells expressing TPC2-mRFP or $TPC2^{K204}$-mRFP were loaded with Fura-2, and fluorescence changes were imaged using an inverted microscope during superfusion. Single-cell microinjections were performed using pipettes back-filled with an intracellular solution supplemented with or without 1 μM NAADP.

Electrophysiology

Currents were recorded in the inside-out configuration from macropatches excised from the plasma membrane of HEK-293T transiently expressing $TPC2^{L11A/L12A}$ or the indicated mutant. Data were acquired using an AxoPatch 200B amplifier (Molecular Devices) and pClamp10.2 suite (Molecular Devices). Records were filtered at 2 kHz and digitized at 10 kHz using Digidata 1440 A (Molecular Devices). ClampFit 10.2 was used for offline analysis of data. Currents were evoked by voltage ramps from −100 to +100 mV over 400 ms repeated at 5-s intervals from a holding potential of 0 mV. Patch pipettes were pulled from thick-walled, filamented borosilicate glass capillaries (Shutter Instrument) using Narishige PC-10 vertical puller, and fire-polished using a Narishige MF-830 microforge (Digitimer Ltd.).

For experiments with symmetrical Na^+, the pipette (luminal) solution contained 145 mM NaCl, 5 mM KCl, 1 mM $MgCl_2$, 2 mM $CaCl_2$, 10 mM Hepes, and 10 mM MES (pH adjusted to 4.6 using methane sulfonic acid). The bath (cytosolic) solution contained 145 mM NaCl, 5 mM KCl, and 10 mM Hepes (pH adjusted to 7.2 using NaOH). For experiments under bi-ionic conditions, the pipette (luminal) solution contained 105 mM $CaCl_2$, 5 mM Hepes, and 5 mM MES (pH adjusted to 4.6 using methane sulfonic acid). The bath (cytosolic) solution contained 160 mM NaCl and 5 mM Hepes (pH adjusted to 7.2 using NaOH). Pipettes had a resistance of 1 to 3 megohms when filled with the pipette solution. Liquid junction potentials were estimated using pClamp 10 and corrected as described previously (45).

TPC2-A1-N (10 μM), TPC2-A1-P (10 μM), $PI(3,5)P_2$ (10 μM diC8 form; Echelon Biosciences), and NAADP (100 nM; Tocris) were applied to the bath solution of excised macropatches via an eight-channel pressurized perfusion system controlled by Valve-Link 8.2 controller (AutoMate Scientific). All electrophysiological recordings were made at room temperature (21° to 23°C).

Statistics

Parametric tests were performed using an unpaired *t* test or one-way analysis of variance (ANOVA). Nonparametric tests were performed using Kruskal-Wallis. All data were analyzed using Prism 9 (GraphPad Software) where *n* refers to the number of independent experiments. $*P < 0.05$, $**P < 0.01$, $***P < 0.001$, and $****P < 0.0001$.

Graphics

Cartoons were created using BioRender.

Supplementary Material

Refer to Web version on PubMed Central for supplementary material.

Acknowledgments:

We thank W. Andrews (UCL) for assistance with molecular biology, Y. Jiang (UT Southwestern) for plasmids, and A. Agrotis (UCL) for helpful comments.

Funding:

This work was supported by BBSRC grants BB/T015853/1 (to S.P.) and BB/W01551X/1 (to T.R. and S.P.); NIH grants GM088790 (to J.S.M. and S.P.) and P30 DA 012429 (to E.B.); DFG grants GR4315/2-2, GR4315/4-1, SFB/TRR152 P04, SFB1328 A21, and GRK2338 P08 (to C.G.); and BR 1034/7-1 (to F.B.) and a PhD studentship from AstraZeneca (to M.E.). For the purpose of open access, the author has applied a Creative Commons Attribution (CC BY) licence to any author accepted manuscript version arising.

REFERENCES AND NOTES

1. Galione A, A primer of NAADP-mediated Ca2+ signalling: From sea urchin eggs to mammalian cells. Cell Calcium 58, 27–47 (2015). [PubMed: 25449298]
2. Churchill GC, Okada Y, Thomas JM, Genazzani AA, Patel S, Galione A, NAADP mobilizes Ca^{2+} from reserve granules, lysosome-related organelles, in sea urchin eggs. Cell 111, 703–708 (2002). [PubMed: 12464181]
3. Calcraft PJ, Ruas M, Pan Z, Cheng X, Arredouani A, Hao X, Tang J, Rietdorf K, Teboul L, Chuang KT, Lin P, Xiao R, Wang C, Zhu Y, Lin Y, Wyatt CN, Parrington J, Ma J, Evans AM, Galione A, Zhu MX, NAADP mobilizes calcium from acidic organelles through two-pore channels. Nature 459, 596–600 (2009). [PubMed: 19387438]
4. Brailoiu E, Churamani D, Cai X, Schrlau MG, Brailoiu GC, Gao X, Hooper R, Boulware MJ, Dun NJ, Marchant JS, Patel S, Essential requirement for two-pore channel 1 in NAADP-mediated calcium signaling. J. Cell Biol 186, 201–209 (2009). [PubMed: 19620632]
5. Zong X, Schieder M, Cuny H, Fenske S, Gruner C, Rötzer K, Griesbeck O, Harz H, Biel M, Wahl-Schott C, The two-pore channel TPCN2 mediates NAADP-dependent Ca^{2+}-release from lysosomal stores. Pflugers Arch 458, 891–899 (2009). [PubMed: 19557428]
6. Patel S, Function and dysfunction of two-pore channels. Sci. Signal 8, re7 (2015). [PubMed: 26152696]
7. Rahman T, Cai X, Brailoiu GC, Abood ME, Brailoiu E, Patel S, Two-pore channels provide insight into the evolution of voltage-gated Ca^{2+} and Na^{+} channels. Sci. Signal 7, ra109 (2014). [PubMed: 25406377]
8. Brailoiu E, Rahman T, Churamani D, Prole DL, Brailoiu GC, Hooper R, Taylor CW, Patel S, An NAADP-gated two-pore channel targeted to the plasma membrane uncouples triggering from amplifying Ca^{2+} signals. J. Biol. Chem 285, 38511–38516 (2010). [PubMed: 20880839]
9. Aley PK, Mikolajczyk AM, Munz B, Churchill GC, Galione A, Berger F, Nicotinic acid adenine dinucleotide phosphate regulates skeletal muscle differentiation via action at two-pore channels. Proc. Natl. Acad. Sci. U.S.A 107, 19927–19932 (2010). [PubMed: 21041635]
10. Patel S, Kilpatrick BS, Two-pore channels and disease. Biochim. Biophys. Acta Mol. Cell Res 1865, 1678–1686 (2018). [PubMed: 29746898]
11. Lin-Moshier Y, Keebler MV, Hooper R, Boulware MJ, Liu X, Churamani D, Abood ME, Walseth TF, Brailoiu E, Patel S, Marchant JS, The two-pore channel (TPC) interactome unmasks isoform-specific roles for TPCs in endolysosomal morphology and cell pigmentation. Proc. Natl. Acad. Sci. U.S.A 111, 13087–13092 (2014). [PubMed: 25157141]
12. Sakurai Y, Kolokoltsov AA, Chen CC, Tidwell MW, Bauta WE, Klugbauer N, Grimm C, Wahl-Schott C, Biel M, Davey RA, Two-pore channels control Ebola virus host cell entry and are drug targets for disease treatment. Science 347, 995–998 (2015). [PubMed: 25722412]
13. Grimm C, Holdt LM, Chen CC, Hassan S, Müller C, Jörs S, Cuny H, Kissing S, Schröder B, Butz E, Northoff B, Castonguay J, Luber CA, Moser M, Spahn S, Lüllmann-Rauch R, Fendel C, Klugbauer N, Griesbeck O, Haas A, Mann M, Bracher F, Teupser D, Saftig P, Biel M, Wahl-Schott C, High susceptibility to fatty liver disease in two-pore channel 2-deficient mice. Nat. Commun 5, 4699 (2014). [PubMed: 25144390]
14. Kilpatrick BS, Eden ER, Hockey LN, Yates E, Futter CE, Patel S, An endosomal NAADP-sensitive two-pore Ca^{2+} channel regulates ER-endosome membrane contact sites to control growth factor signaling. Cell Rep 18, 1636–1645 (2017). [PubMed: 28199837]
15. Li ZH, King TP, Ayong L, Asady B, Cai X, Rahman T, Vella SA, Coppens I, Patel S, Moreno SNJ, A plastid two-pore channel essential for inter-organelle communication and growth of Toxoplasma gondii. Nat. Commun 12, 5802 (2021). [PubMed: 34608145]

16. Marchant JS, Patel S, Questioning regulation of two-pore channels by NAADP. Messenger 2, 113–119 (2013). [PubMed: 24829847]

17. Lin-Moshier Y, Walseth TF, Churamani D, Davidson SM, Slama JT, Hooper R, Brailoiu E, Patel S, Marchant JS, Photoaffinity labeling of nicotinic acid adenine dinucleotide phosphate (NAADP) targets in mammalian cells. J. Biol. Chem 287, 2296–2307 (2012). [PubMed: 22117075]

18. Walseth TF, Lin-Moshier Y, Jain P, Ruas M, Parrington J, Galione A, Marchant JS, Slama JT, Photoaffinity labeling of high affinity nicotinic acid adenine dinucleotide phosphate (NAADP)-binding proteins in sea urchin egg. J. Biol. Chem 287, 2308–2315 (2012). [PubMed: 22117077]

19. Walseth TF, Lin-Moshier Y, Weber K, Marchant JS, Slama JT, Guse AH, Nicotinic acid adenine dinucleotide 2'-phosphate (NAADP) binding proteins in T-lymphocytes. Messenger (Los. Angel.) 1, 86–94 (2012). [PubMed: 24829846]

20. Ruas M, Davis LC, Chen CC, Morgan AJ, Chuang KT, Walseth TF, Grimm C, Garnham C, Powell T, Platt N, Platt FM, Biel M, Wahl-Schott C, Parrington J, Galione A, Expression of Ca^{2+}-permeable two-pore channels rescues NAADP signalling in TPC-deficient cells. EMBO J 34, 1743–1758 (2015). [PubMed: 25872774]

21. Gunaratne GS, Brailoiu E, He S, Unterwald EM, Patel S, Slama JT, Walseth TF, Marchant JS, Essential requirement for JPT2 in NAADP-evoked Ca^{2+} signaling. Sci. Signal 14, (2021).

22. Roggenkamp HG, Khansahib I, Hernandez C LC., Zhang Y, Lodygin D, Krüger A, Gu F, Möckl F, Löhndorf A, Wolters V, Woike D, Rosche A, Bauche A, Schetelig D, Werner R, Schlüter H, Failla AV, Meier C, Fliegert R, Walseth TF, Flügel A, Diercks BP, Guse AH, HN1L/JPT2: A signaling protein that connects NAADP generation to Ca^{2+} microdomain formation. Sci. Signal 14, eabd5605 (2021). [PubMed: 33758061]

23. Zhang J, Guan X, Shah K, Yan J, Lsm12 is an NAADP receptor and a two-pore channel regulatory protein required for calcium mobilization from acidic organelles. Nat. Commun 12, 4739 (2021). [PubMed: 34362892]

24. Patel S, Gregori M, Yuan Y, Teaming with NAADP. Sci. Signal 14, eabh2798 (2021). [PubMed: 33758059]

25. Marchant JS, Gunaratne GS, Cai X, Slama JT, Patel S, NAADP binding proteins find their identity. Trends Biochem. Sci 47, 235–249 (2022). [PubMed: 34810081]

26. Wang X, Zhang X, Dong XP, Samie M, Li X, Cheng X, Goschka A, Shen D, Zhou Y, Harlow J, Zhu MX, Clapham DE, Ren D, Xu H, TPC proteins are phosphoinositide-activated sodium-selective ion channels in endosomes and lysosomes. Cell 151, 372–383 (2012). [PubMed: 23063126]

27. She J, Guo J, Chen Q, Zeng W, Jiang Y, Bai XC, Structural insights into the voltage and phospholipid activation of the mammalian TPC1 channel. Nature 556, 130–134 (2018). [PubMed: 29562233]

28. She J, Zeng W, Guo J, Chen Q, Bai XC, Jiang Y, Structural mechanisms of phospholipid activation of the human TPC2 channel. eLife 8, e45222 (2019). [PubMed: 30860481]

29. Cang C, Bekele B, Ren D, The voltage-gated sodium channel TPC1 confers endolysosomal excitability. Nat. Chem. Biol 10, 463–469 (2014). [PubMed: 24776928]

30. Schieder M, Rotzer K, Bruggemann A, Biel M, Wahl-Schott CA, Characterization of two-pore channel 2 (TPCN2)-mediated Ca^{2+} currents in isolated lysosomes. J. Biol. Chem 285, 21219–21222 (2010). [PubMed: 20495006]

31. Pitt SJ, Funnell TM, Sitsapesan M, Venturi E, Rietdorf K, Ruas M, Ganesan A, Gosain R, Churchill GC, Zhu MX, Parrington J, Galione A, Sitsapesan R, TPC2 is a novel NAADP-sensitive Ca^{2+}-release channel, operating as a dual sensor of luminal pH and Ca^{2+}. J. Biol. Chem 285, 24925–24932 (2010). [PubMed: 20547763]

32. Gerndt S, Chen CC, Chao YK, Yuan Y, Burgstaller S, Scotto Rosato A, Krogsaeter E, Urban N, Jacob K, Nguyen ONP, Miller MT, Keller M, Vollmar AM, Gudermann T, Zierler S, Schredelseker J, Schaefer M, Biel M, Malli R, Wahl-Schott C, Bracher F, Patel S, Grimm C, Agonist-mediated switching of ion selectivity in TPC2 differentially promotes lysosomal function. eLife 9, e54712 (2020). [PubMed: 32167471]

33. Yuan Y, Jaślan D, Rahman T, Bolsover SR, Arige V, Wagner LE II, Abrahamian C, Tang R, Keller M, Hartmann J, Rosato AS, Weiden EM, Bracher F, Yule DI, Grimm C, Patel S, Segregated cation

flux by TPC2 biases Ca^{2+} signaling through lysosomes. Nat. Commun 13, 4481 (2022). [PubMed: 35918320]

34. Gunaratne GS, Brailoiu E, Kumar S, Yuan Y, Slama JT, Walseth TF, Patel S, Marchant JS, Convergent activation of two pore channels through unique NAADP-binding proteins. Sci. Signal 16, eadg0485 (2023). [PubMed: 37607218]
35. Jha A, Ahuja M, Patel S, Brailoiu E, Muallem S, Convergent regulation of the lysosomal two-pore channel-2 by Mg^{2+}, NAADP, $PI(3,5)P_2$ and multiple protein kinases. EMBO J 33, 501–511 (2014). [PubMed: 24502975]
36. Penny CJ, Vassileva K, Jha A, Yuan Y, Chee X, Yates E, Mazzon M, Kilpatrick BS, Muallem S, Marsh M, Rahman T, Patel S, Mining of Ebola virus entry inhibitors identifies approved drugs as two-pore channel pore blockers. Biochim. Biophys. Acta Mol. Cell Res 1866, 1151–1161 (2019). [PubMed: 30408544]
37. Zhang X, Chen W, Li P, Calvo R, Southall N, Hu X, Bryant-Genevier M, Feng X, Geng Q, Gao C, Yang M, Tang K, Ferrer M, Marugan JJ, Xu H, Agonist-specific voltage-dependent gating of lysosomal two-pore Na^+ channels. eLife 8, e51423 (2019). [PubMed: 31825310]
38. Patel S, Churamani D, Brailoiu E, NAADP-evoked Ca^{2+} signals through two-pore channel-1 require arginine residues in the first S4-S5 linker. Cell Calcium 68, 1–4 (2017). [PubMed: 29129203]
39. Shimomura T, Hirazawa K, Kubo Y, Conformational rearrangements in the second voltage sensor domain switch PIP_2- and voltage-gating modes in two-pore channels. Proc. Natl. Acad. Sci. U.S.A 120, e2209569120 (2023). [PubMed: 36724253]
40. Lee HC, Zhao YJ, Resolving the topological enigma in Ca^{2+} signaling by cyclic ADP-ribose and NAADP. J. Biol. Chem 294, 19831–19843 (2019). [PubMed: 31672920]
41. Scotto Rosato A, Krogsaeter EK, Jaślan D, Abrahamian C, Montefusco S, Soldati C, Spix B, Pizzo MT, Grieco G, Böck J, Wyatt A, Wünkhaus D, Passon M, Stieglitz M, Keller M, Hermey G, Markmann S, Gruber-Schoffnegger D, Cotman S, Johannes L, Crusius D, Boehm U, Wahl-Schott C, Biel M, Bracher F, de Leonibus E, Polishchuk E, Medina DL, Paquet D, Grimm C, TPC2 rescues lysosomal storage in mucolipidosis type IV, Niemann-Pick type C1, and batten disease. EMBO Mol. Med 14, e15377 (2022). [PubMed: 35929194]
42. Lam AJ, St-Pierre F, Gong Y, Marshall JD, Cranfill PJ, Baird MA, McKeown MR, Wiedenmann J, Davidson MW, Schnitzer MJ, Tsien RY, Lin MZ, Improving FRET dynamic range with bright green and red fluorescent proteins. Nat. Methods 9, 1005–1012 (2012). [PubMed: 22961245]
43. Guo J, Zeng W, Jiang Y, Tuning the ion selectivity of two-pore channels. Proc. Natl. Acad. Sci. U.S.A 114, 1009–1014 (2017). [PubMed: 28096396]
44. Kilpatrick BS, Eden ER, Hockey LN, Futter CE, Patel S, Methods for monitoring lysosomal morphology. Methods Cell Biol 126, 1–19 (2015). [PubMed: 25665438]
45. Barry PH, JPCalc, a software package for calculating liquid junction potential corrections in patch-clamp, intracellular, epithelial and bilayer measurements and for correcting junction potential measurements. J. Neurosci. Methods 51, 107–116 (1994). [PubMed: 8189746]

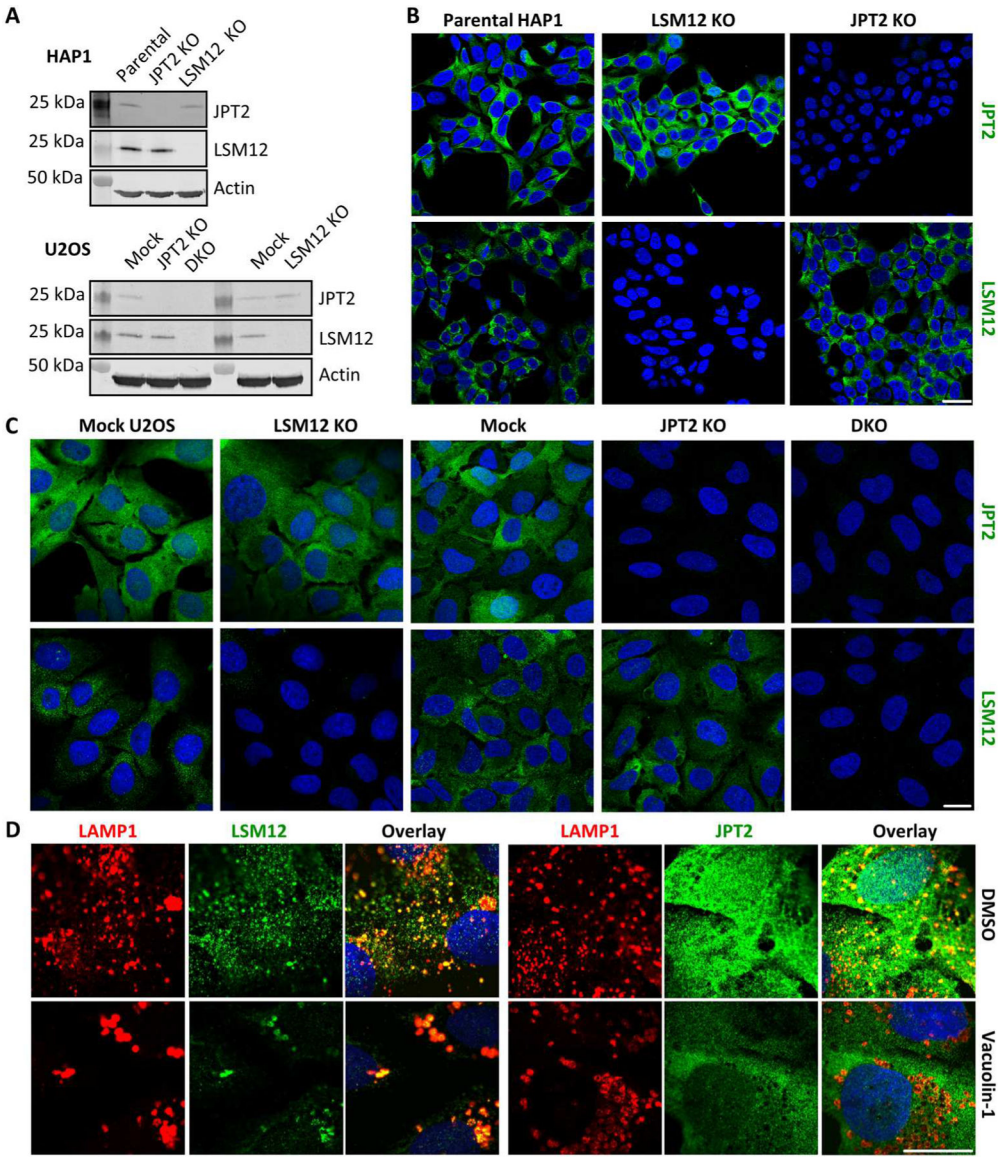

Fig. 1. Subcellular distribution and knockout of NAADP-binding proteins in mammalian cells.

(**A**) Western blot analyses of parental, JPT2 knockout (KO), and LSM12 KO HAP1 cells and mock KO, JPT2 KO, LSM12 KO, and double-knockout (DKO) U2OS cells using antibodies directed against JPT2 or LSM12. Actin is a positive control. Blot is representative of $n = 2$ to 4 independent experiments. (**B** and **C**) Immunofluorescence showing JPT2 and LSM12 in HAP1 (B) and U2OS cells (C). Nuclei were stained with DAPI (blue). The two mock samples shown in (C) differ in passage number. (**D**) Immunofluorescence showing JPT2 and LSM12 and the late endosome and lysosomal marker LAMP1 in U2OS cells treated with either dimethyl sulfoxide (DMSO) or vacuolin-1. Scale bars, 20 μm. Images are representative of $n = 3$ independent experiments.

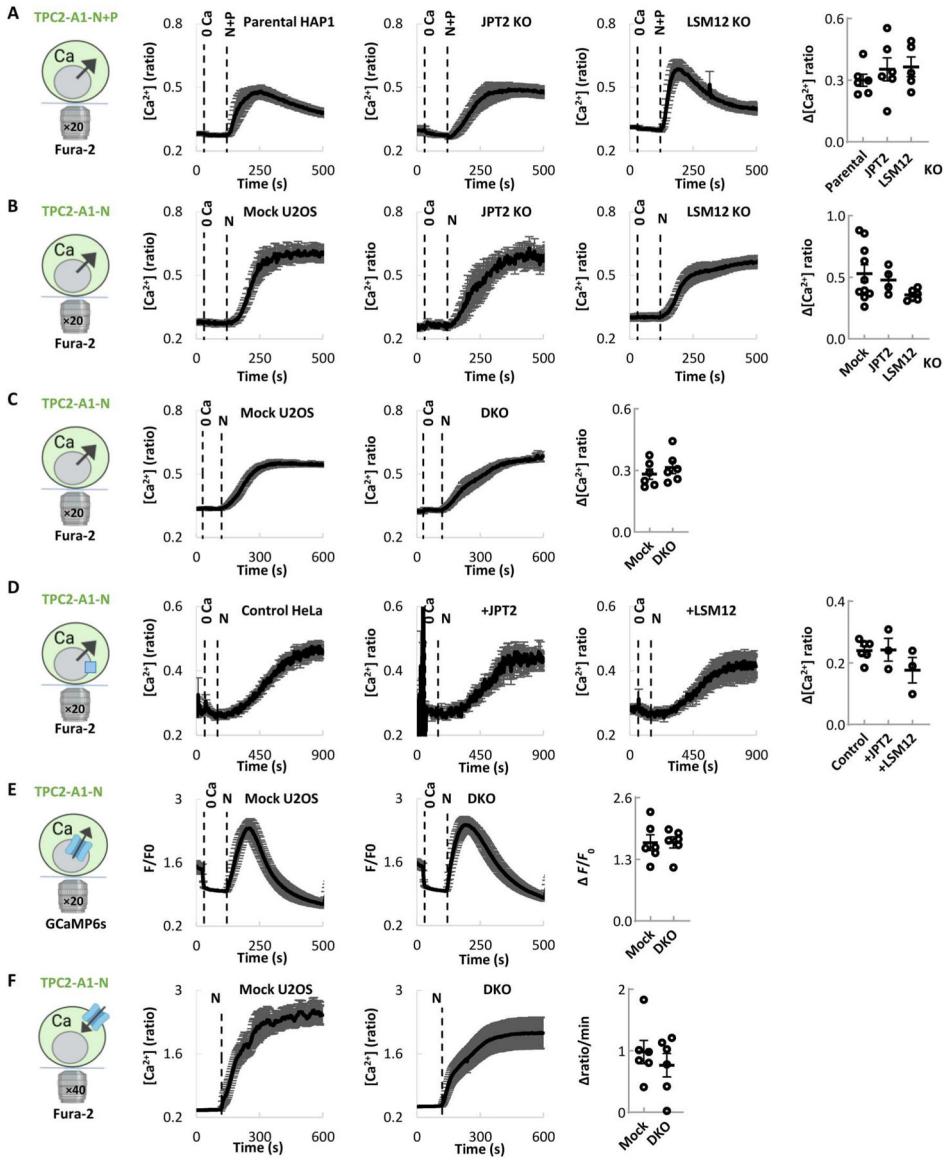

Fig. 2. The NAADP functional mimetic TPC2-A1-N mediates Ca^{2+} signals independently of NAADP-binding proteins.

Quantification of intracellular Ca^{2+} release and Ca^{2+} influx in various cell lines either loaded with the Ca^{2+} indicator Fura-2 or expressing $TPC2^{GCaMP6s}$ and treated with TPC2-A1-N alone or in combination with TPC2-A1-P (TPC2-A1-N+P). Intracellular Ca^{2+} was measured as the change in the Fura-2 fluorescence ratio or GCaMP6s fluorescence intensity, and each trace is the fluorescence response recorded from a cell population (means ± SEM). Graphs show the maximal change in signal in each experimental group (means ± SEM), and each point represents the mean response from an independent experiment. (**A**) Intracellular Ca^{2+} release in parental, JPT2 knockout (KO), and LSM12 KO HAP1 cells treated with TPC2-A1-N+P. n = 6 for parental, 6 for JPT2 KO, and 5 for LSM12 KO. One-way ANOVA followed by Dunnett's post hoc test. (**B**) Intracellular Ca^{2+} release in in mock KO, JPT2 KO, and LSM12 KO U2OS cells treated with TPC2-A1-N. n = 10 for mock KO, 4 for JPT2 KO, and 6 for LSM12 KO. One-way ANOVA followed by Dunnett's post hoc test.

(**C**) Intracellular Ca^{2+} release in mock KO and JPT2 and LSM12 double-knockout (DKO) U2OS cells treated with TPC2-A1-N. $n = 6$ for each group. Unpaired *t* test. (**D**) Intracellular Ca^{2+} release in HeLa cells overexpressing JPT2-mRuby2 or LSM12-mRuby2 (blue square in diagram) and treated with TPC2-A1-N. $n = 6$ for control, 3 for JPT2, and 3 for LSM12. One-way ANOVA followed by Dunnett's post hoc test. (**E** and **F**) Intracellular Ca^{2+} release (E) and Ca^{2+} influx (F) in mock KO and DKO U2OS cells expressing lysosome-localized $TPC2^{GCaMP6s}$ (E) or plasma membrane–localized $TPC2^{L11A/L12A}$ (F). In (E), Ca^{2+} release was measured using the change in GCaMP6s fluorescence. $n = 6$ for mock KO and 6 for DKO (E); 6 for mock KO and 6 for DKO (F). Unpaired *t* test.

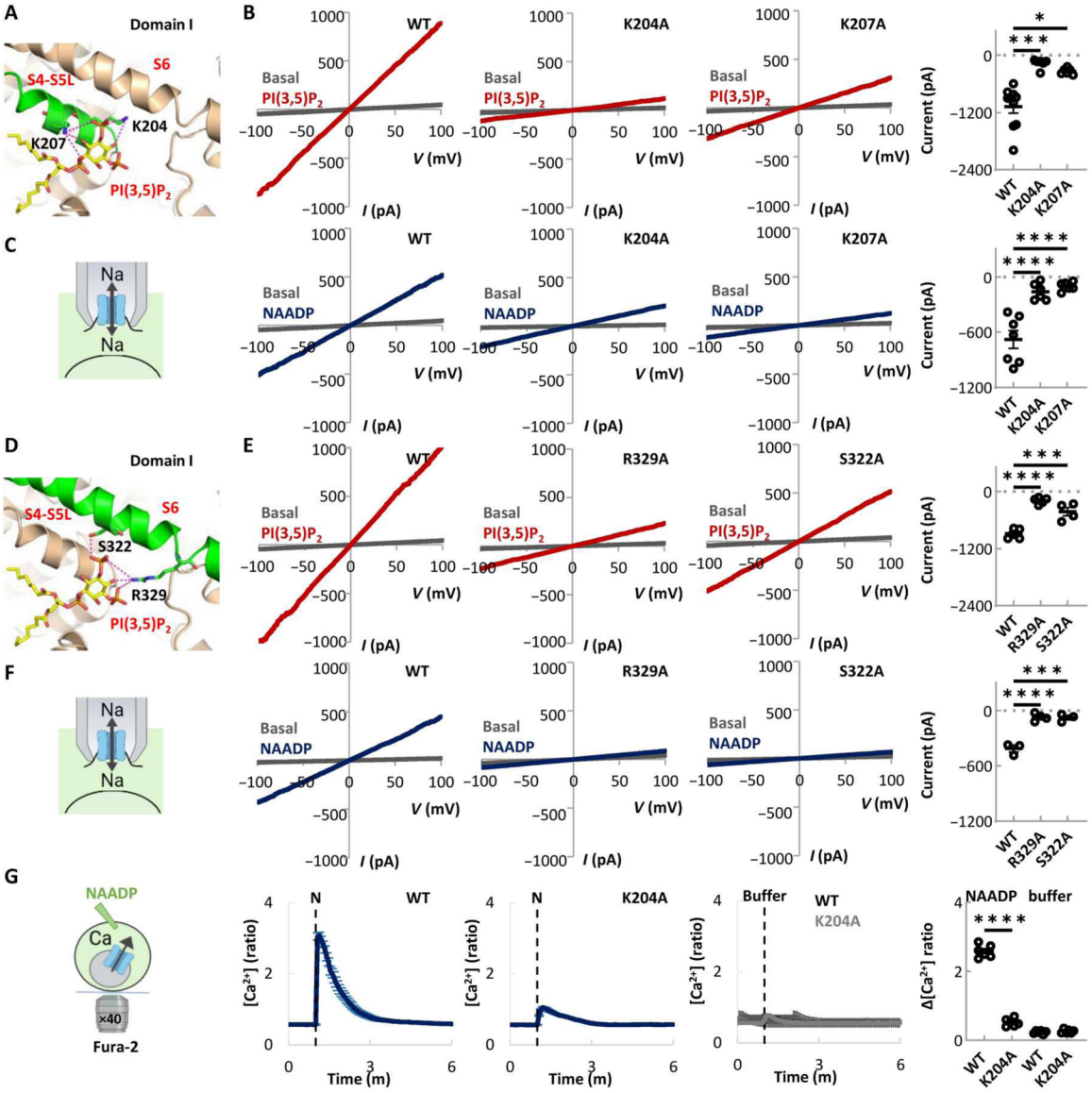

Fig. 3. Activation of TPC2 by NAADP requires the PI(3,5)P_2 binding site.

(**A**) Structure of human TPC2 [Protein Data Bank (PDB): 6NQ1] highlighting basic residues in the S4-S5 linker of domain I involved in PI(3,5)P_2 binding. (**B**) Currents in HEK cells transiently expressing wild-type (WT), K204A, or K207A form of plasma membrane–localized TPC2$^{L11A/L12A}$ and stimulated with PI(3,5)P_2, as measured by patch clamping using symmetrical Na^+ solutions. The graph shows the inward Na^+ currents at −100 mV in response to PI(3,5)P_2 (means ± SEM; $n = 10$ for WT, 6 each for K204A and K207A). ***$P < 0.0001$ and *$P < 0.05$ (Kruskal-Wallis test). (**C**) Currents from HEK cells transiently expressing the WT, K204A, or K207A form of TPC2$^{L11A/L12A}$ and stimulated with NAADP, as measured by patch clamping using symmetrical Na^+ solutions. The graph shows the inward Na^+ currents at −100 mV in response to NAADP (means ± SEM; $n = 7$ for WT, 6 each for K204A and K207A). ****$P < 0.0001$ (one-way ANOVA followed by Dunnett's post hoc test). (**D**) Structure of human TPC2 (PDB: 6NQ0) highlighting residues in S6 of

domain I involved in $PI(3,5)P_2$ binding. (**E**) Currents in HEK cells transiently expressing the WT, R329A, or S322A form of $TPC2^{L11A/L12A}$ and stimulated with $PI(3,5)P_2$, as measured by patch clamping using symmetrical Na^+ solutions. The graph shows the inward Na^+ currents at −100 mV in response to $PI(3,5)P_2$ (means ± SEM; $n = 5$ for WT, 5 for R329A, and 4 for S322A). ****$P < 0.0001$ and ***$P < 0.001$ (one-way ANOVA followed by Dunnett's post hoc test). (**F**) Currents from HEK cells transiently expressing the WT, R329A, or S322A form of $TPC2^{L11A/L12A}$ and stimulated with NAADP as measured by patch clamping using symmetrical Na^+ solutions. The graph shows the inward Na^+ currents at −100 mV in response to NAADP (means ± SEM; $n = 3$ for WT, 4 for R329A, and 3 for S322A). ****$P < 0.0001$ and ***$P < 0.001$ (one-way ANOVA followed by Dunnett's post hoc test). (**G**) Quantification of intracellular Ca^{2+} release in U2OS cells transiently expressing TPC2 or $TPC2^{K204A}$ and stimulated with NAADP. Intracellular Ca^{2+} release was measured as the change in the Fura-2 fluorescence ratio. Control injection of buffer alone is shown. The graph shows the maximal change in fluorescence ratio in response to NAADP or buffer (means ± SEM; $n = 6$ for each experimental group). ****$P < 0.0001$ (unpaired t test).

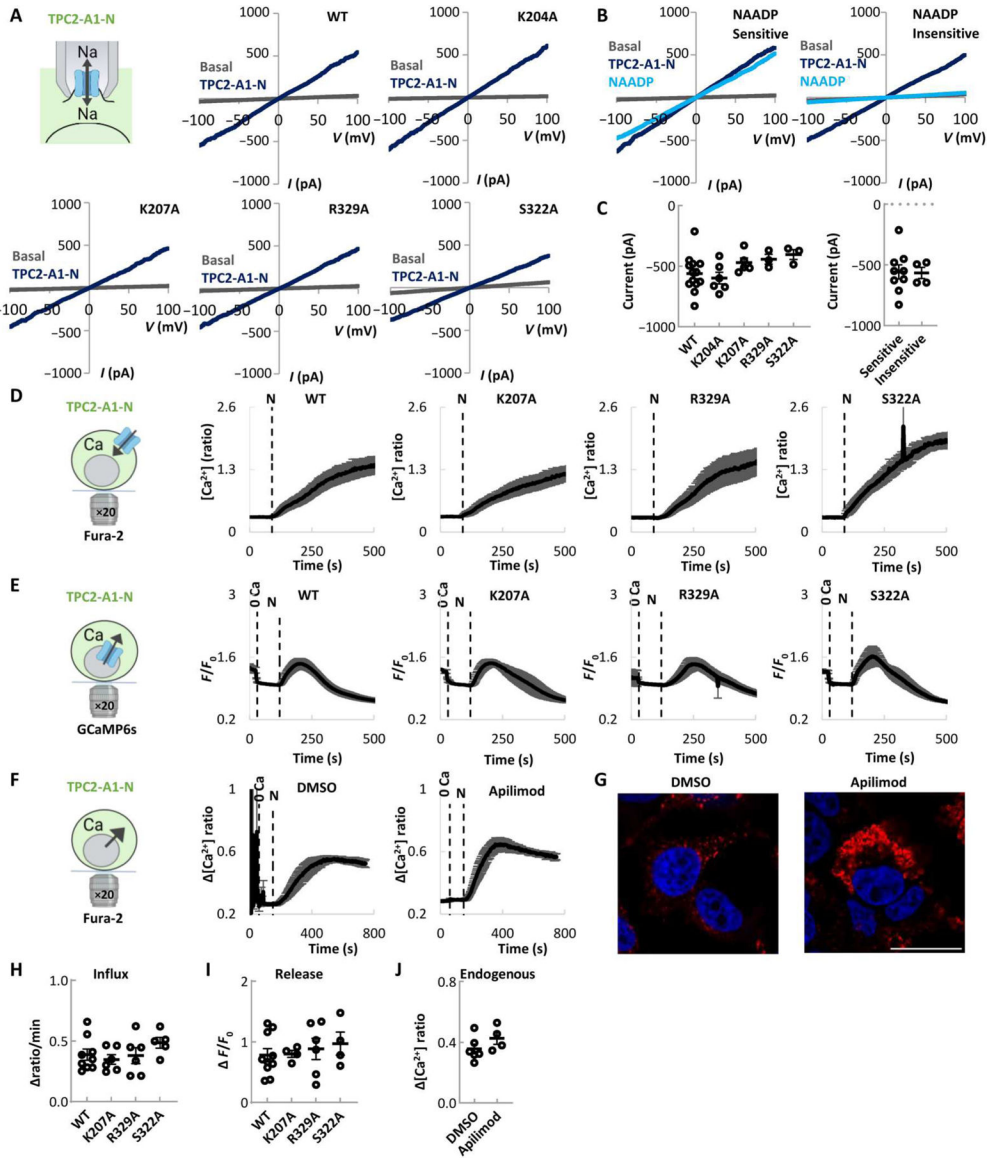

Fig. 4. Activation of TPC2 by TPC2-A1-N is independent of PI(3,5)P_2.

(**A**) Currents in HEK cells transiently expressing WT TPC2$^{L11A/L12A}$ or the indicated PI(3,5)P_2 binding site mutant and stimulated with TPC2-A1-N, as measured by patch clamping. (**B**) Examples of recordings from macropatches that were responsive to both NAADP and TPC2-A1-N (left) or to TPC2-A1-N only (right). (**C**) Summary of data in (A) and (B). (means ± SEM; n = 13 for WT, 6 for K204A, 5 for K207A, 3 for R329A, 3 for S322A, 9 for sensitive, and 4 for insensitive). One-way ANOVA followed by Dunnett's post hoc test (left) and unpaired t test (right). (**D**) Quantification of Ca^{2+} influx by Fura-2 imaging in HeLa cells expressing WT TPC2$^{L11A/L12A}$ or the indicated PI(3,5)P_2 binding site mutant and stimulated with TPC2-A1-N (means ± SEM). (**E**) Quantification of intracellular Ca^{2+} release by GCaMP6s imaging in HeLa cells expressing WT TPC2-GCaMP6s or the indicated PI(3,5)P_2 binding site mutant and stimulated with TPC2-A1-N (means ± SEM). (**F**) Quantification of intracellular Ca^{2+} release by Fura-2 imaging in HeLa cells treated

with DMSO or apilimod. (means ± SEM). (**G**) Immunofluorescence showing LAMP1 (red) in HeLa cells after treatment with DMSO or the PIKfyve inhibitor apilimod. Nuclei were stained with DAPI (blue). Images are representative of $n = 3$ independent experiments. (**H**) Summary of data from (D) (means ± SEM) where each point represents the mean response from an independent experiment ($n = 9$ for WT, 6 for K207A, 6 for R329A, and 5 for S322A). One-way ANOVA followed by Dunnett's post hoc test. (**I**) Summary of data from (E) (means ± SEM) where each point represents the mean response from an independent experiment ($n = 10$ for WT, 4 for K207A, 6 for R329A, and 4 for S322A). One-way ANOVA followed by Dunnett's post hoc test. (**J**) Summary of data from (F) (means ± SEM) where each point represents the mean response from an independent experiment ($n = 6$ for control and 4 for Apilimod). Unpaired *t* test.

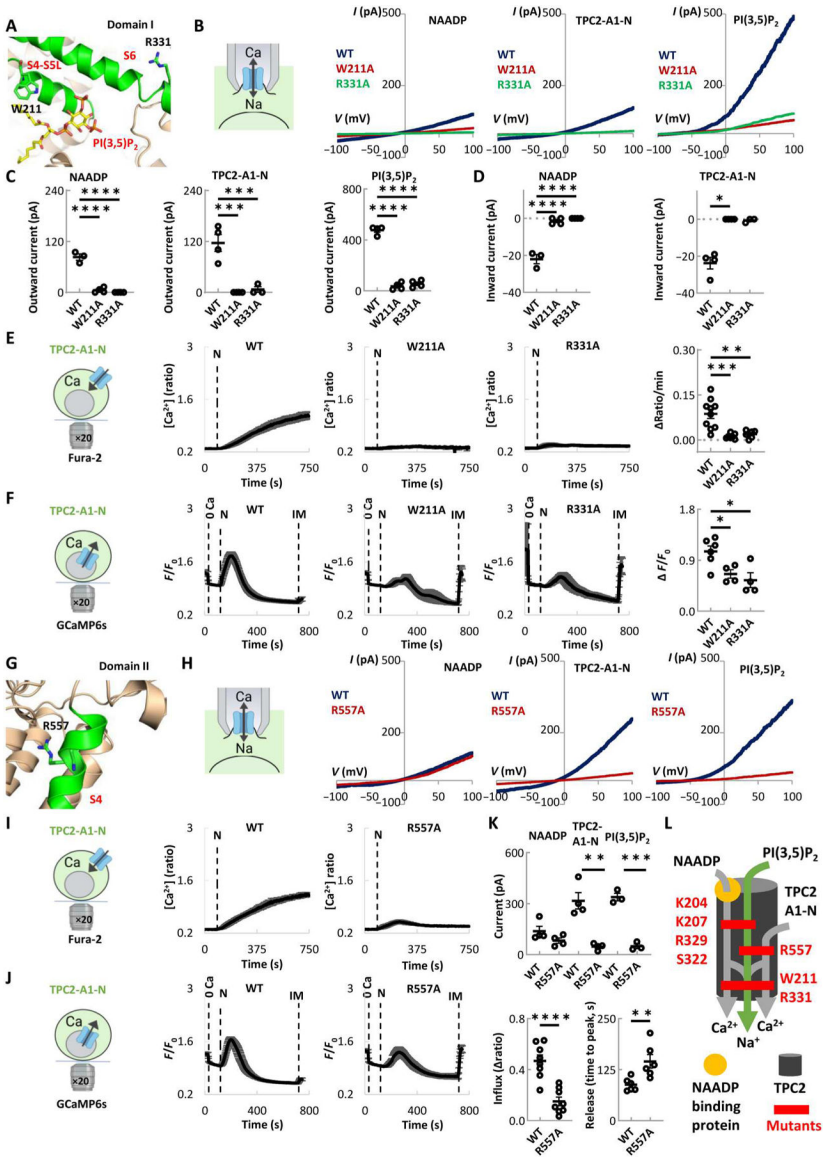

Fig. 5. Residues outside the PI(3,5)P_2 binding site required for agonist action.

(**A**) Structure of human TPC2 (PDB: 6NQ0) highlighting residues neighboring the PI(3,5)P_2 binding site. (**B**) Currents, measured by patch clamping with bi-ionic Na^+ and Ca^{2+} solutions, in HEK cells transiently expressing the WT, W211A, or R331A form of plasma membrane–localized $TPC2^{L11A/L12A}$ and stimulated with NAADP, PI(3,5)P_2 or TPC2-A1-N. (**C**) Summary of data in (B) quantifying the outward Na^+ currents at +100 mV in response to NAADP (means ± SEM; $n = 3$ for control, 4 for W211A, and 4 for S331A), TPC2-A1-N (means ± SEM; $n = 4$ for control, 4 for W211A, and 3 for S331A), or PI(3,5)P_2 (means ± SEM; $n = 4$ for control, 4 for W211A, and 4 for S331A). ****$P < 0.0001$ and ***$P < 0.001$ (one-way ANOVA followed by Dunnett's post hoc test). (**D**) Summary of data in (B) quantifying the inward Ca^{2+} currents at −100 mV in response to NAADP (means ± SEM; $n = 3$ for control, 4 for W211A, and 4 for S331A) or TPC2-A1-N (means ± SEM; $n = 4$ for control, 4 for W211A, and 3 for S331A). ****$P < 0.0001$ (one-way ANOVA followed

by Dunnett's post hoc test). *$P < 0.05$ (Kruskal-Wallis test). (**E**) Quantification of Ca^{2+} influx by Fura-2 imaging in HeLa cells expressing the indicated form of $TPC2^{L11A/L12A}$ and stimulated with TPC2-A1-N. Data are summarized in the graph (means ± SEM; n = 10 for control, 7 for W211A, and 6 for S331A). ***$P < 0.001$ and **$P < 0.01$ (one-way ANOVA followed by Dunnett's post hoc test). (**F**) Quantification of intracellular Ca^{2+} release by GCaMP6s imaging in HeLa cells expressing the indicated form of $TPC2^{GCaMP6s}$ and stimulated with TPC2-A1-N. Ionomycin (IM) was added at the end of the experiment. Data are summarized in the graph. (means ± SEM; n = 6 for control, 4 for W211A, and 4 for S331A). *$P < 0.05$ (one-way ANOVA followed by Dunnett's post hoc test). (**G**) Structure of human TPC2 (PDB: 6NQ0) highlighting Arg^{557} in the voltage sensing region in domain II. (**H**) Currents, measured by patch clamping with bi-ionic Na^+ and Ca^{2+} solutions, in HEK cells transiently expressing the WT or R557A form of $TPC2^{L11A/L12A}$ and stimulated with NAADP, $PI(3,5)P_2$, or TPC2-A1-N. (**I**) Quantification of Ca^{2+} influx by Fura-2 imaging in HeLa cells expressing WT or R557A $TPC2^{L11A/L12A}$ and stimulated with TPC2-A1-N. (**J**) Quantification of intracellular Ca^{2+} release by GCaMP6s imaging in HeLa cells expressing the WT or R557A form of $TPC2^{GCaMP6s}$ and stimulated with TPC2-A1-N. (**K**) Graphs summarizing the data from (H) to (J). The top graph shows the outward Na^+ currents at +100 mV in response to NAADP (means ± SEM; n = 4 for control and 4 for R557A), TPC2-A1-N (means ± SEM; n = 4 for control and 4 for R557A), and $PI(3,5)P_2$ (means ± SEM; n = 3 for control and 3 for R557A). **$P < 0.01$ and ***$P < 0.001$ (unpaired t test). The bottom graphs show the magnitude of Ca^{2+} influx at a set time (330 s) (means ± SEM; n = 8 for control and 8 for R557A) (left) and the time to peak for Ca^{2+} release (means ± SEM; n = 6 for control and 6 for R557A) (right) in response to TPC2-A1-N. ****$P < 0.0001$ (unpaired t test). **$P < 0.01$ (Kruskal-Wallis test). (**L**) Schematic illustrates the divergent mechanisms that mediate polymodal activation and ion selectivity switching in TPC2. Activation of TPC2 by NAADP requires NAADP-binding proteins. Mutations in the $PI(3,5)P_2$ binding site (K204A, K207A, R329A, and S322A) block NAADP but not TPC2-A1-N action, whereas a mutation in the cryptic voltage-sensing domain (R557A) blocks TPC2-A1-N but not NAADP action. Both sets of mutations block channel activation by $PI(3,5)P_2$. Additional mutations (W211A and R331A) block channel activation by all three agonists.